Role of polymers in the physical and chemical stability of amorphous solid dispersion: A case study of carbamazepine

Dongyue Yu , Jinghan Li , Hanxun Wang , Hao Pan , Ting Li , Tianshi Bu , Wei Zhou , Xiangrong Zhang

PII: S0928-0987(21)00387-0
DOI: https://doi.org/10.1016/j.ejps.2021.106086
Reference: PHASCI 106086

To appear in: *European Journal of Pharmaceutical Sciences*

Received date: 21 August 2021
Revised date: 30 October 2021
Accepted date: 27 November 2021

Please cite this article as: Dongyue Yu , Jinghan Li , Hanxun Wang , Hao Pan , Ting Li , Tianshi Bu , Wei Zhou , Xiangrong Zhang , Role of polymers in the physical and chemical stability of amorphous solid dispersion: A case study of carbamazepine, *European Journal of Pharmaceutical Sciences* (2021), doi: https://doi.org/10.1016/j.ejps.2021.106086

Role of polymers in the physical and chemical stability of amorphous solid dispersion: A case study of carbamazepine

Dongyue Yu [a, 1], Jinghan Li [b, 1, #], Hanxun Wang [c], Hao Pan [d], Ting Li [b], Tianshi Bu [b], Wei Zhou [e] *, Xiangrong Zhang [b] *

a. Department of Pharmaceutical Sciences, School of Pharmacy, University of Maryland, Baltimore, 20 North Pine Street, Baltimore, Maryland, 21201, USA

b. Shenyang Pharmaceutical University, 103 Wenhua Road, Shenyang, 110016, China

c. Key Laboratory of Structure-Based Drug Design & Discovery, Ministry of Education, Shenyang Pharmaceutical University, Shenyang, 110016, China

d. School of Pharmaceutical Science, Liaoning University, 66 Chongshan Mid Road, Shenyang, 110036, China

e. Hydrogeological and Geothermal Geological Key Laboratory of Qinghai Province, Survey of Hydrogeology and Engineering Geology and Environmental Geology in Qinghai Province, No. 4 Sujiahewan, Xining, 810008, China

*Corresponding authors: Department of Pharmaceutics, College of Pharmacy, University of Minnesota-Twin Cities, 308 SE Harvard St, Minneapolis, Minnesota, 55455, USA

[1]These authors contributed equally to this work.

ABSTRACT

Incorporating the amorphous drug in polymeric components has been demonstrated as a feasible approach to enhance the bioavailability of poorly water-soluble drugs. The objective of this study was to investigate the role of polymers in the stability of amorphous solid dispersion (ASD) by evaluating the drug-polymer interaction, microenvironmental pH, and stability of ASD. Carbamazepine (CBZ), a Biopharmaceutics Classification System Class II compound, was utilized as a model drug. Polyvinylpyrrolidone (PVP), poly(1-vinylpyrrolidone-co-vinyl acetate) (PVPVA), polyacrylic acid (PAA), and hydroxypropyl methylcellulose (HPMCAS) were selected as model polymers. CBZ ASDs were characterized by X-ray diffraction (XRD), differential scanning calorimetry (DSC), thermogravimetric analysis (TGA), Fourier transform infrared (FTIR) spectroscopy, and dissolution studies. Molecular modeling was conducted to understand the strength of interaction between CBZ and each polymer. FTIR spectroscopy and molecular modeling results show that the interaction between CBZ and PAA is the strongest among all the ASDs, as PAA is an acidic polymer with the potential to form strong hydrogen bonding with CBZ. Besides, hydrophobic interaction is detected between CBZ and HPMCAS. CBZ-PAA and CBZ-HPMCAS ASDs reveal better physical stability than CBZ-PVP and CBZ-PVPVA ASDs under 40 °C/75% RH for 8 weeks. However, CBZ-PAA ASD shows chemical degradation after stability testing due to its acidic microenvironmental pH. This paper shows that strong intermolecular interactions between CBZ and polymers contribute to the physical stability

of the ASDs. Additionally, acidic polymers yield an acidic microenvironment pH of the ASDs that causes chemical degradation during storage. Hence, a balance between the ability of a given polymer to promote physical stability and chemical stability may need to be considered.

Keywords

Amorphous solid dispersion (ASD), intermolecular interaction, microenvironmental pH, physical stability, chemical stability, carbamazepine (CBZ)

INTRODUCTION

Amorphization is one of the most effective approaches to improve the solubility of Biopharmaceutics Classification System (BCS) class II and IV drugs. However, the amorphous drug itself has the risk of recrystallization because of its high free energy. One of the most commonly used approaches to stabilize the amorphous drug is to molecularly disperse the drug in a polymeric matrix and form an amorphous solid dispersion (ASD) (Kothari, Ragoonanan, and Suryanarayanan 2015). A physically stable ASD can be obtained by increasing the polymer content, selecting polymer with higher molecular weight, or the ability to form strong drug-polymer intermolecular interactions: for instance, nifedipine-polyvinylpyrrolidone (PVP) ASDs, the crystallization onset time increased with polymer content (Mistry et al. 2015), and the increase of PVP molecular weight resulted in higher the viscosity of the indomethacin-PVP ASDs and improved the physical stability (Mohapatra et al. 2017). Compared with polyacrylic acid (PAA) and hydroxypropyl methylcellulose (HPMCAS), PVP formed stronger hydrogen bonding with nifedipine, which could effectively inhibit drug recrystallization (Kothari, Ragoonanan, and Suryanarayanan 2015). However, in addition to physical stability, chemical degradation could be a problem for high-energy amorphous molecules. In the previous study, amorphous quinapril hydrochloride degraded rapidly with a cyclization reaction (Guo, Byrn, and Zografi 2000). As hot-melt extrusion is one of the most commonly used techniques for ASD preparation, approaches have been developed to improve the chemical stability of ASD at elevated temperatures. Studies showed that *in situ* drug-excipient interaction played an essential role in chemically stabilizing the amorphous drug during hot-melt extrusion. For example, meloxicam interacted with meglumine with ionic interaction in the copovidone matrix during extrusion, and the ternary polymeric ASD showed enhanced stability (Haser et al. 2018). Besides, the combination of Soluplus® and HPMCAS enhanced the physical and chemical stability of the carbamazepine extrudes by introducing intermolecular interactions (Alshahrani et al. 2015).

In addition to the high energy state and the thermal-induced chemical instability of the amorphous solids, microenvironmental pH (or surface acidity, solid-state acidity) can be another critical factor causing chemical degradation, especially during long-term storage (Badawy and Hussain 2007). It has been reported that the solid-state stability of theophylline cocrystals was highly relevant to the acidity of the coformers under accelerated conditions (Koranne et al. 2019). The acidification of the lyophilized products caused sucrose inversion, which implied the fluctuation of the microenvironmental pH could be detrimental to pH-sensitive compounds (Enxian et al. 2009). However, few studies have shown the role of microenvironmental pH of ASDs on the chemical stability of the drug substance during storage. The microenvironmental

pH can be determined using: 1) slurry pH method: the pH of the concentrated suspension reflects the surface acidity of the suspended particles; 2) indicator dye-sorption method: the absorption peaks of the indicator dye measured with UV-visible diffuse reflectance spectrum provides a measurement of Hammett acidity function, which reflects the microenvironment pH of the samples.

In this work, PVP, poly (1-vinylpyrrolidone-co-vinyl acetate) (PVPVA), HPMCAS L grade, and PAA were selected as the model polymers to generate different microenvironmental pH of the ASDs. Among these polymers, PVP and PVPVA are neutral polymers with carbonyl groups as the proton acceptors (Rumondor and Taylor 2010). HPMCAS is a synthetic amphipathic polymer derived from cellulose. The L, M, and H grades HPMCAS differ in the contents of acetyl, succinoyl, methoxyl, and hydroxypropyl functional groups (Sarabu et al. 2020). PAA is an acidic polymer with a pK_a of 4.5 (Mistry et al. 2015). The carboxylic acid groups of HPMCAS and PAA determine their acidic property and act as proton donors. Carbamazepine (CBZ), an antiepileptic drug attributed to BCS class II, was used as the model compound (Sethia and Squillante 2004). It is an extremely weak base (pK_a: 13.9) with four anhydrous polymorphs and commercialized in form III (Grzesiak et al. 2003). CBZ can potentially form different drug-polymer interactions with the selected model polymers, which can influence the physical stability of the ASDs. Moreover, we speculated that the microenvironmental pH of the ASDs impacts the chemical stability of amorphous CBZ after storage under stressed conditions. The aim of this study is to investigate the role of drug-polymer interaction and microenvironmental pH in the physical and chemical stability of the CBZ ASDs. We hypothesized that 1) strong intermolecular interactions between CBZ and polymers contributed to the physical stability of the ASDs and 2) acidic polymers yielded an acidic microenvironment of the ASDs could potentially accelerate chemical degradation during storage.

EXPERIMENTAL

Materials

Figure 1 shows the chemical structures of CBZ and polymers. CBZ (purity, 98%) was purchased from Allbio Pharm Co., Ltd (Suzhou, China), and CBZ Pharmacopeia of the People's Republic of China (ChP) reference standard (purity = 99%, lot number: 100142-201105) was obtained from Xinyang Laiyao Biological Technology Co., Ltd (Xinyang, China). Kollidon® 30 (PVP K30, M_w ~ 40000 g/mol) and Kollidon® VA64 (PVPVA 64, M_w ~ 35000 to 51000 g/mol, m:n = 6:4) were purchased from BASF Corp (Shanghai, China). HPMCAS (L grade, M_w ~ 13000 g/mol) and PAA (M_w ~ 1800 g/mol) were purchased from Aladdin Bio-Chem Technology Co., Ltd (Shanghai, China). Solvents of HPLC grade were provided by Shandong Yuwang Tech Reagent Company (Shandong, China).

Methods

Sample Preparation

CBZ and each polymer of the same mass were dissolved in methanol and evaporated using a vacuum rotary evaporator (RE-2000, Henan Lanphan Technology Co., Ltd, Henan, China) at 55 °C. For further analysis, the prepared samples were dried in a vacuum desiccator (DZF-6503, Qixin Scientific Instrument, Shanghai, China) for 48 hours and stored in a sealed aluminum package at -20 °C. The amorphous CBZ was prepared by melting the crystalline drug in a sealed DSC pan above melting temperature, then quenching it on a precooled metal pan at -20 °C. The physical mixtures (PMs) were prepared by gently grinding the drug-polymer mixture using a mortar and pestle.

Differential Scanning Calorimetry

A DSC (DSC 1, Mettler Toledo, Greifensee, Switzerland) was used to study the thermal events of the samples upon heating at a rate of 10 °C/min from 0 °C to 220 °C under a nitrogen gas flow of 30 mL/min. About 2 to 5 mg of each sample was sealed in hermetical aluminum pans, with an empty pan as a reference.

Thermogravimetric analysis

Thermogravimetric analysis (TGA) was performed with a TA instrument Hi-Res TGA (TA Instruments, New Castle, Delaware, USA). About 5 mg of sample was heated in alumina crucible from room temperature to 300 °C at a heating rate of 10 °C/min under a 30 mL/min nitrogen flow.

X-ray Diffractometry

An X-ray diffractometer (D/MAX-3C, Rigaku Co., Kyoto, Japan) was used to determine the solid form of the ASDs. The samples were analyzed in the range of 5–40° 2θ with a step size of 0.02° 2θ per second using a voltage of 56 kV and a current of 35 mA.

Fourier Transform Infrared Spectroscopy

The intermolecular interactions were studied using Fourier transform infrared (FTIR) spectroscopy (IN10, Thermo Fisher, USA). The resolution was 4 cm^{-1} with 64 scans in the range from 4000 to 600 cm^{-1}. The peaks were plotted using OriginLab 2018 (OriginaLab Corporation, Massachusetts, USA).

Molecular modeling

Molecular modeling, a useful tool to study ligand-protein interaction, has also been developed to study the drug-polymer interaction in ASDs (Han et al. 2019; Li et al. 2020). In this work, polymer structure coordinates were first prepared by ChemAxon Marvin Sketch (ChemAxon Ltd., Budapest, Hungary). Given the chemical complexity of the polymer structures, the degree of substitution of the polymer was simplified. Initially modeled molecules were then optimized by classical molecular docking with AMBER algorithm (AMBER 2018, University of California, California, USA). Polymers were performed with antechamber modules in AmberTools18 under GAFF force field in the modeling process. The polymer systems, including 6 HPMCAS, 11 PAA, 4 PVP, and 4 PVPVA polymer chains, were individually used to build a molecular cluster, neutralized by Na^+ and Cl^- and optimized in vacuum for 20ns. Then, these clusters were used for

molecular docking study. Ligand molecule CBZ was also build by ChemAxon Marvin Sketch, and further ligand minimization was performed by Sybyl (Tripos Inc., Missouri, USA). A molecular docking study was provided by Glide 9.7 embedded in Schrodinger Suite (Schrödinger, LLC, New York, USA). The glide grid was set big enough for each polymer structure to include the whole polymer structure to find a better binding mode of CBZ. In the ligand docking module, precision was set as standard precision, ligand sampling as flexible, and each polymer should give out no less than 20 docking results. Finally, the docking results with the best docking score for each CBZ-polymer combination were selected for further discussion in the result section.

Physical stability test

The physical stability tests were carried out at 40 °C in desiccators containing anhydrous calcium sulfate and a saturated sodium chloride solution to realize dry and 75% relative humidity (RH) conditions in darkness.

Microenvironmental pH measurement

While the acidity measured using an indicator dye depends on the type of the indicator, the slurry pH method provides a rapid and convenient measurement of microenvironment pH and is applied in the current project (Pudipeddi et al. 2008). Dried samples at the amount of about 40% (w/w) excess of the CBZ saturated solubility were added to distilled water and mixed using a shaker (TS-500, Haimen Kylin-Bell Lab Instruments Co., Ltd., Jiangsu, China) at room temperature. The pH values were measured using a PB-10 pH electrode (Sartorius AG, Göttingen, Germany). Equilibrium was reached after 20 minutes that the pH values do not show significant changes with further shaking.

High-performance Liquid Chromatography

Detection and quantification were carried out with a Shimadzu LC-20AT prominence system controller (Shimazu Scientific Instruments, Kyoto, Japan) for CBZ. The InertSustain^{TM} C18 (250×4.6 mm, 5 μm) column (GL Sciences Inc., Tokyo, Japan) was used. The mobile phase consisted of methanol/water (45/55) (v/v) at a flow rate of 1.0 ml/min using detection wavelength at 254 nm, and the injection volume was 10 μL. Data were integrated and analyzed using the Shimadzu Class-VP Chromatography Laboratory Automated Software system.

***In vitro* Dissolution Study**

The dissolution test followed the USP apparatus 2 method (708-DS Dissolution Apparatus, Agilent technologies, California, USA) at the paddle speed of 100 rpm. Crystalline CBZ and ASDs with equivalent CBZ content were dispersed in 900 mL of pH 1.2 and 6.8 buffers at 37 °C with sink condition maintained. 3 mL aliquots were collected at fixed time points and filtered with 0.45 μm nylon membrane (Changde Bkmam Biotechnology Co., Ltd., Hunan, China). The samples were analyzed at 284 nm using a UV spectrophotometer (UV-6, Shanghai Metash Instruments Co., Ltd., Shanghai, China).

RESULTS

X-ray Diffractometry

According to the XRD results (Figure 2), the neat CBZ is a form III polymorph (Lim, Yu, and Hoag 2021). The diffraction peaks disappear in the XRD patterns of the prepared ASDs, which means all the CBZ ASDs are amorphous (Figure 2).

Thermal Analysis

CBZ form III and I are a monotropic pair of polymorphs. Based on the DSC result, the crystallization of CBZ form I (176.7 °C) happens right after the melting of form III (175.3 °C), and form I finally melts at 191.5 °C. Besides glass transitions, PVP and PVPVA ASDs do not show any other thermal events. The glass transition temperatures (T_gs) of PVP, PVPVA, HPMCAS, and PAA ASDs are 94.7 °C, 72.5 °C, 65.5 °C, and 104.5 °C, which are typical indicators for their amorphous state (Figure 3). Although a higher T_g value does not indicate a more stable amorphous solid, according to a "rule of thumb," amorphous solids are supposed to be stored at "T_g-50K" (Hancock and Zografi 1997). In our case, CBZ ASDs with higher T_gs can have better physical stability during storage. However, endotherms occur in the DSC thermograms of HPMCAS and PAA ASDs above 150 °C (Figure 3). According to Figure 4 and S1, pure polymers are stable and do not show other thermal events except for glass transitions upon heating to 200 °C. The crystalline CBZ and polymers start losing weight around 220 °C, and the weight loss of the PVP and PVPVA ASDs start at similar temperatures to the polymers (Figure 4 and S2). However, the degradation of HPMCAS and PAA ASDs happened at lower temperatures compared with the crystalline CBZ and the polymers, which indicates that the prepared ASDs using HPMCAS and PAA are less stable than the crystalline CBZ and the polymers upon heating (Figure 4). Besides, the first derivation of the TGA curves showed that the decomposition temperatures of the HPMCAS and PAA ASDs are similar to temperatures of the DSC endotherms above 150 °C (Figure S2). A previous study has found that the decomposition processes of CBZ started even before the melting of form I polymorph (Dołęga, Zieliński, and Osiecka-Drewniak 2019). Our DSC and TGA results explained that the decomposition was exacerbated as CBZ form ASDs with acidic polymers HPMCAS and PAA during heating.

Fourier Transform Infrared Spectroscopy

In the IR spectrum of neat CBZ, the peak at 3465 cm^{-1} is attributed to the N-H stretching of the primary amine. The peak at 1676 cm^{-1} represents the C=O stretching. C=C stretching and N-H deformation result in the split peaks at 1606 and 1595 cm^{-1}. The peak at 1385 cm^{-1} is attributed to C-H bending (Figure 5) (Rustichelli et al. 2000). After amorphization, N-H stretching peaks in the neat CBZ and physical mixture disappear, and the split peaks at 1606 and 1595 cm^{-1} merge into one broad peak at the lower wavenumber, which may imply the primary amine of CBZ form hydrogen bonding with the polymers after preparing ASDs (Figure S3) (Sethia and Squillante 2004).

The strong peak at 1676 cm^{-1} in the physical mixture of CBZ and PVP is the combination of the C=O stretching of the drug and polymer. In a previous study, the author pointed out that there might be hydrogen bonding between the CBZ amino group and the PVP carbonyl group.

However, we do not observe significant changes (< 2 cm^{-1}) in the wavenumber of the carbonyl group around 1676 cm^{-1}, which means such interaction might be very weak (Figure 5a) (Sethia and Squillante 2004). PVPVA has two C=O stretching peaks at 1734 and 1676 $cm^{-1}$are attributed to the carbonyl groups of vinyl acetate and vinylpyrrolidone, respectively (Rumondor and Taylor 2010). In the CBZ-PVPVA ASD, the C=O stretching of vinyl acetate and the second C=O stretching peak almost remain at the same wavenumber (< 2 cm^{-1}), which indicates weak drug-polymer interaction (Figure 5b). The intense peak at 1740 cm^{-1} in the FTIR spectrum of HPMCAS is attributed to the C=O stretching, which almost remains constant in wavenumber (< 2 cm^{-1}) after forming ASD with CBZ. Interestingly, the C=O stretching peak of CBZ blueshifts from 1676 to 1682 cm^{-1} probably results from the dissociation of the CBZ drug-drug interaction due to the steric hindrance effect of HPMCAS (Figure 5c). Similarly, the weaker drug-drug interaction in the CBZ form I compared with form III yields a higher wavenumber of the C=O stretching peak (Rustichelli et al. 2000; Lim, Yu, and Hoag 2021). Other ASD studies also showed that the hydrophobic forces, instead of hydrogen bonding, benefited the physical stability of HPMCAS ASDs (Chen et al. 2018). When the carboxylic acid groups form cyclic dimers, it will result in a strong C=O stretching peak at 1705 cm^{-1}. However, the non-interacted carboxylic acid groups in PAA reveal a C=O stretching peak at higher wavenumber (ElMiloudi et al. 2005). In our study, the blue shift of the PAA C=O stretching peak to 1709 cm^{-1} probably results from the partial dissociation of the carboxylic acid dimers due to the presence of CBZ. More importantly, the C=O stretching of CBZ redshifts from 1678 to 1641 cm^{-1} (highlighted with an arrow), indicating strong hydrogen bonding between the CBZ amide group and PAA carboxylic acid (Figure 5d) (Taylor and Zografi 1997; Limwikrant et al. 2012).

Molecular Modeling

Although the FTIR spectroscopy results reveal weak drug-polymer interaction in CBZ-PVP and CBZ-PVPVA ASDs and strong hydrogen bonds in the CBZ-PAA ASD, some interactions are challenging to study due to the complexity of spectroscopy in the amorphous state. For example, the increased number of energy states of amorphous CBZ compared with its crystalline form may also result in peak "disappear" because of peak broadening, so the absence of primary amino group stretching peaks in the FTIR spectroscopy study may not indicate an intermolecular interaction (Figure S4). Moreover, non-directional hydrophobic interactions generally do not result in apparent phenomena in spectroscopy. Therefore, a molecular modeling experiment was carried out to understand the drug-polymer interaction qualitatively (Figure S5). The GlideScore provides an empirical function of ligand-protein binding affinity, which includes terms taking account for different interactions, especially suitable for systems that contain hydrophobic forces. A more negative value represents a more tightly bonded ligand-protein system (Friesner et al. 2006). In our case, the score could help us understand the overall affinity between CBZ and polymers because of various drug-polymer interactions. ASDs containing PVP, PVPVA, HPMCAS, and PAA have scores of -6.95, -8.35, -7.46, -10.68, respectively, which means the integral drug-polymer interaction between CBZ and PAA is the strongest. In contrast, the interaction between CBZ and PVP is the weakest among all the model ASDs.

According to the molecular modeling study, the amide group of CBZ does not interact with PVP, which supports our IR results. However, because of the presence of hydrophobic dibenzazepine ring in CBZ, PVP interacts with CBZ by weak hydrophobic forces with the bond distance ranging from 4.20 to 4.73 Å (Figure 6a). CBZ in the PVPVA matrix also shows similar hydrophobic forces (bond distance: 3.77 to 4.05 Å). In addition, the amino group can act as a proton donor and form hydrogen-bond with the carbonyl group of PVPVA (Figure 6b). Although HPMCAS contains carboxylic acid groups, molecular modeling does not reveal interactions between CBZ and its carboxylic acid groups. The carboxylic acid groups in HPMCAS tended to form a hydrogen bond with other functional groups on the polymer chain, such as carbonyl groups. Instead, the CBZ amide group forms a hydrogen bond with its hydroxyl group and ether oxygen. However, we suspect the actual situation in the CBZ-HPMCAS systems may be more complicated as the polymers have multiple hydrogen donors and acceptors. It is worth noticing that there is a strong hydrophobic interaction (bond distance: 2.14 Å) between CBZ and HPMCAS, which may contribute to the improved stability of the CBZ-HPMCAS ASD (Figure 6c). Moreover, the interactions between CBZ and PAA are supposed to be the strongest among all the ASDs, with three types of hydrogen bonds between the amide and carboxylic acid groups (Figure 6d). Based on the above results, we can conclude that: 1) PVP weakly interact with CBZ via hydrophobic forces; 2) there are weak hydrophobic forces and hydrogen bonding in CBZ-PVPVA ASD; 3) CBZ could be stabilized by both hydrogen bonding and strong hydrophobic forces in the HPMCAS ASD; 4) there is strong hydrogen bond in CBZ-PAA ASD.

Physical Stability

Neat CBZ form III did not transform to its dihydrate form under 40 °C/75% RH (data not shown), which was also supported by other studies (Rahman et al. 2011). Under 40 °C dry condition, all the CBZ ASDs maintained in the amorphous state after 8 weeks (Figure 7a). According to the XRD results, CBZ-PVP and CBZ-PVPVA ASDs recrystallized into CBZ form III under 40 °C/75% RH condition after 8 weeks, while the ASDs containing HPMCAS and PAA remained physically stable (Figure 7b). This could be explained by the presence of strong hydrogen bonding or hydrophobic forces for CBZ-HPMCAS and CBZ-PAA ASDs. Among all the hydrophilic polymers, PAA showed stronger drug-polymer interactions with CBZ compared with PVP and PVPVA. On the other hand, as an amphipathic polymer, HPMCAS stabilizes the drug with strong hydrophobic force. However, undesirable changes in the appearance of PAA samples were observed (Figure 8), indicating that chemical degradation might happen.

Chemical Stability

The freshly prepared CBZ-HPMCAS ASD is an off-white powder, while the other ASDs are pure white powder (Figure 8). The morphology of neat CBZ did not change after storage at 40 °C dry and 40 °C/75% RH conditions. Although the CBZ ASDs containing PVP and PVPVA recrystallized after storing at 40 °C/75% RH for 8 weeks, the powder became paste but remained white. Although the CBZ-PAA ASD remained physically stable after storage, it turned yellow at 40 °C dry and 40 °C/75% RH conditions after 8 weeks (Figure 8). The degradation mechanism of CBZ is rather complex: it could be influenced by heat, light, oxygen, acidity, solvent, and ionic species. The C=C on the azepine ring is highly active to a series of polar reactions, possibly

resulting in the formation of eslicarbazepine, oxcarbazepine, 10, 11-dihydro-10, 11-dihydroxycarbamazepine, licarbazepine, etc. Some of degrades are yellow or orange and vulnerable to further degradation (Daniele et al. 2017; Monteagudo et al. 2015). From Table 1, we found that the acidity of the polymer determines the microenvironmental pHs of the ASDs. PAA ASD shows the most acidic microenvironmental pH among all the ASDs.

HPLC was used to quantify the drug degradation after the stability test. While the purity of neat CBZ is 98%, the initial CBZ content in the ASDs containing PVP, PVPVA, PAA and HPMCAS were 47.86 ± 0.16%, 44.61 ± 0.01%, 46.79 ± 0.01%, and 46.54 ± 0.06%, respectively (Table 2). Accelerated conditions at elevated temperatures with the presence of oxygen caused slight degradation of CBZ. In general, CBZ ASDs at 40 °C did not experience significant chemical degradation despite their high energy amorphous state. CBZ remained chemically stable in CBZ-PVP and CBZ-PVPVA ASDs, even though they recrystallized to CBZ form III during storage under 40 °C/75 % RH condition. However, CBZ-PAA ASD showed around 13% degradation at 40 °C/75 % RH (Table 2). While all the samples were stored at the same open conditions (40 °C or 40 °C/75 % RH), the only difference is the microenvironmental pH determined by the polymer matrix. The above phenomena and the thermal analysis results (Figures 3 and 4) possibly indicated that the acidic microenvironment exacerbated the degradation process. Other papers also found similar results that acidic conditions accelerated the decomposition of CBZ under ultrasonic irradiation (with dissolved air) or with the presence of other oxidants (Mohapatra et al. 2014; Deng et al. 2013).

In vitro dissolution study

The dissolution of the ASDs was evaluated using a USP apparatus 2 method under sink conditions at pH 1.2 and 6.8 buffers. Crystalline CBZ dissolved slightly faster in the pH 1.2 than pH 6.8 (Figure 9). Under the studied pH conditions, CBZ-PVP and CBZ-PVPVA ASDs showed improved dissolution rate and drug release compared with the neat CBZ (Figure 9). Although the acidic PAA dissolved better at pH 6.8, the hydrophilic nature of PAA also provides good solubility in acidic conditions. However, the dissolution of CBZ-HPMCAS ASD is highly pH-dependent: it did not show much dissolution improvement at pH 1.2, while nearly 95% of the drug was released after 60 min at pH 6.8. Similar phenomena were also observed in other studies (Solanki et al. 2019; Monschke and Wagner 2020).

DISCUSSION

As an approach to enhance dissolution and oral bioavailability, many strategies have been applied to prevent drug recrystallization of ASD during storage. Increasing the polymer content may not always be the most desirable way to enhance ASD stability since it can cause a dose burden during administration. Selecting a polymer that can form robust drug-polymer interaction can also stabilize the drug in the amorphous state even at relatively low polymer content (Mistry et al. 2015). Most of the studies emphasize the stabilization effect of directional strong intermolecular interaction, especially ionic interaction and hydrogen bonding. However, emerging numbers of ASDs are formulated with HPMCAS, an amphipathic polymer, using spray drying and hot-melt extrusion. Although some HPMCAS ASD studies lack clear evidence of

directional intermolecular interaction, they showed excellent physical stability under accelerated conditions. Hydrophobic forces characterized using the solution and solid-state NMR in HPMCAS ASD can prevent drug recrystallization (Ueda et al. 2013; Honick et al. 2020). We found that strong hydrophobic force and hydrogen bonding in the CBZ-HPMCAS ASD contributed to the enhanced physical stability of the ASD under 40 °C/75% RH for at least 8 weeks (Figure 6b). Here we want to highlight the importance of hydrophobic forces in the stabilization of ASD, such as HPMCAS, especially under the circumstances that a significant fraction of active pharmaceutical ingredients and new chemical entities are hydrophobic (Frank and Matzger 2019; Singh, Bedi, and Tiwary 2018).

In addition to physical stability, the current study also carried out a chemical stability assessment. Molecules in an amorphous state have higher free energy and are more vulnerable to chemical degradation (Guo, Byrn, and Zografi 2000). In this case, extreme microenvironmental pH can accelerate chemical degradation. PAA forms strong ionic interaction with the basic moiety of drug molecules and stabilizes drugs in amorphous state under tropical conditions (Duggirala et al. 2019; Gui et al. 2021). In our case, PAA also formed strong hydrogen bonds with CBZ. However, the low microenvironmental pH in the PAA ASD induced 13% CBZ degradation at 40 °C/75 % RH after 8 weeks (Table 2). The results highlight the risk of using acidic polymers, such as PAA, for pH-sensitive compounds, especially with moisture and high temperature. As most of the efforts have been made to improve the physical stability of ASD, in this paper, we highlighted that the extreme ASD microenvironmental pH determined by the polymer matrix resulted in drug degradation that could cause undesirable product appearance and potential *in vivo* toxicity.

CONCLUSION

The study prepared and evaluated CBZ ASDs using different polymers, PVP, PVPVA, HPMCAS, and PAA. In addition to FTIR spectroscopy, the molecular modeling experiment could be an ideal supplementary technique to predict the drug-polymer interaction, especially hydrophobic forces. The strong intermolecular interaction, including hydrogen bonding and hydrophobic forces, contributed to the excellent physical stability of the HPMCAS and PAA ASDs. However, our work pointed out that, despite the dissolution advantage and improved physical stability, the microenvironmental pH determined by the acidic polymers could result in undesirable chemical degradation during storage. Our work highlights the importance of the rational selection of the polymer during ASD formulation development based on dissolution performance, physical and chemical stability.

Creadit author statement

Dongyue Yu[1]: Conceptualization, Methodology, Investigation, Writing, Reviewing, Editing.

Jinghan Li[1]: Conceptualization, Methodology, Investigation, Writing, Reviewing, Editing.

Hanxun Wang: Methodology, Investigation, Writing, Reviewing, Editing (section of molecular modeling).

Hao Pan: Methodology, Investigation, Reviewing (section of thermal analysis and X-ray diffractometry).

Ting Li: Methodology, Investigation, Writing (section of sample preparation and dissolution)

Tianshi Bu: Methodology, Investigation (section of thermal analysis and X-ray diffractometry).

Wei Zhou*: Conceptualization, Methodology, Investigation, Writing, Reviewing, Editing, Resources (Fourier transform infrared spectroscopy and high-performance liquid chromatography), Supervision.

Xiangrong Zhang*: Conceptualization, Methodology, Writing, Reviewing, Editing, Resources, Project administration, Funding acquisition, Supervision.

Declaration of Competing Interest

The authors declare no financial interests/personal relationships which may be considered as potential competing interests.

ACKNOWLEDGEMENT

This project is funded by the People's Livelihood Plan Project of Department of Science and Technology of Liaoning Provincial (2021JH2/10300069) and the Department of Education of Liaoning Province (LJKZ0918). The authors would like to thank Qinghai Provincial Drug Inspection and Testing Institute for their support in the experimental work and data analysis. We also thank the Key Laboratory of Structure-Based Drug Design & Discovery in Shenyang Pharmaceutical University for their molecular modeling experiment.

REFERENCE

Alshahrani, Saad M, Wenli Lu, Jun-Bom Park, Joseph T Morott, Bader B Alsulays, Soumyajit Majumdar, Nigel Langley, Karl Kolter, Andreas Gryczke, and Michael A Repka. 2015. Stability-enhanced hot-melt extruded amorphous solid dispersions via combinations of Soluplus® and HPMCAS-HF, *AAPS PharmSciTech*, 16: 824-34.

Badawy, Sherif I Farag, and Munir A Hussain. 2007. Microenvironmental pH modulation in solid dosage forms, *J Pharm Sci*, 96: 948-59.

Chen, Yuejie, Yipshu Pui, Huijun Chen, Shan Wang, Peter Serno, Wouter Tonnis, Linc Chen, and Feng Qian. 2018. Polymer-mediated drug supersaturation controlled by drug–polymer interactions persisting in an aqueous environment, *Mol Pharm*, 16: 205-13.

Daniele, Gaëlle, Maëva Fieu, Sandrine Joachim, Anne Bado-Nilles, Rémy Beaudouin, Patrick Baudoin, Alice James-Casas, Sandrine Andres, Marc Bonnard, and Isabelle Bonnard. 2017. Determination of carbamazepine and 12 degradation products in various compartments of an outdoor aquatic mesocosm by reliable analytical methods based on liquid chromatography-tandem mass spectrometry, *Environ. Sci. Pollut. Res*, 24: 16893-904.

Deng, Jing, Yisheng Shao, Naiyun Gao, Shengji Xia, Chaoqun Tan, Shiqing Zhou, and Xuhao Hu. 2013. Degradation of the antiepileptic drug carbamazepine upon different UV-based advanced oxidation processes in water, *Chem. Eng. J.*, 222: 150-58.

Dołęga, Agnieszka, Piotr M Zieliński, and Natalia Osiecka-Drewniak. 2019. New insight into thermodynamical stability of carbamazepine, *J Pharm Sci*, 108: 2654-60.

Duggirala, Naga Kiran, Jinghan Li, NS Krishna Kumar, Tata Gopinath, and Raj Suryanarayanan. 2019. A supramolecular synthon approach to design amorphous solid dispersions with exceptional physical stability, *Chem. Commun.*, 55: 5551-54.

ElMiloudi, Khaled, Mourad Benygzer, Said Djadoun, Nicolas Sbirrazzuoli, and Serge Geribaldi. 2005. FT - IR Spectroscopy and Hydrogen Bonding Interactions in Poly (styrene - co - methacrylic acid)/Poly (styrene - co - 4 - vinyl pyridine) Blends. *Macromol Symp*, 39-50.

Enxian, Lu, Susan Ewing, Larry Gatlin, Raj Suryanarayanan, and Evgenyi Shalaev. 2009. The effect of bulking agents on the chemical stability of acid-sensitive compounds in freeze-dried formulations: sucrose inversion study, *J Pharm Sci*, 98: 3387-96.

Frank, Derek S, and Adam J Matzger. 2019. Effect of polymer hydrophobicity on the stability of amorphous solid dispersions and supersaturated solutions of a hydrophobic pharmaceutical, *Mol Pharm*, 16: 682-88.

Friesner, Richard A, Robert B Murphy, Matthew P Repasky, Leah L Frye, Jeremy R Greenwood, Thomas A Halgren, Paul C Sanschagrin, and Daniel T Mainz. 2006. Extra precision glide: Docking and scoring incorporating a model of hydrophobic enclosure for protein− ligand complexes, *J. Med. Chem.*, 49: 6177-96.

Grzesiak, Adam L, Meidong Lang, Kibum Kim, and Adam J Matzger. 2003. Comparison of the four anhydrous polymorphs of carbamazepine and the crystal structure of form I, *J Pharm Sci*, 92: 2260-71.

Gui, Yue, Erin C McCann, Xin Yao, Yuhui Li, Karen J Jones, and Lian Yu. 2021. Amorphous Drug–Polymer Salt with High Stability under Tropical Conditions and Fast Dissolution: The Case of Clofazimine and Poly (acrylic acid), *Mol Pharm*, 18: 1364-72.

Guo, Yushen, Stephen R Byrn, and George Zografi. 2000. Physical characteristics and chemical degradation of amorphous quinapril hydrochloride, *J Pharm Sci*, 89: 128-43.

Han, Run, Hui Xiong, Zhuyifan Ye, Yilong Yang, Tianhe Huang, Qiufang Jing, Jiahong Lu, Hao Pan, Fuzheng Ren, and Defang Ouyang. 2019. Predicting physical stability of solid dispersions by machine learning techniques, *J. Control. Release*, 311: 16-25.

Hancock, Bruno C, and George Zografi. 1997. Characteristics and significance of the amorphous state in pharmaceutical systems, *J Pharm Sci*, 86: 1-12.

Haser, Abbe, Tu Cao, Joseph W Lubach, and Feng Zhang. 2018. In situ salt formation during melt extrusion for improved chemical stability and dissolution performance of a meloxicam–copovidone amorphous solid dispersion, *Mol Pharm*, 15: 1226-37.

Honick, Moshe, Sharmila Das, Stephen W. Hoag, Francis X. Muller, Alaadin Alayoubi, Xin Feng, Ahmed Zidan, Muhammad Ashraf, and James E. Polli. 2020. The effects of spray drying, HPMCAS grade, and compression speed on the compaction properties of itraconazole-HPMCAS spray dried dispersions, *Eur. J. Pharm. Sci.*, 155: 105556.

Koranne, Sampada, Joseph F Krzyzaniak, Suman Luthra, Kapildev K Arora, and Raj Suryanarayanan. 2019. Role of coformer and excipient properties on the solid-state stability of theophylline cocrystals, *Cryst. Growth Des.*, 19: 868-75.

Kothari, Khushboo, Vishard Ragoonanan, and Raj Suryanarayanan. 2015. The role of drug–polymer hydrogen bonding interactions on the molecular mobility and physical stability of nifedipine solid dispersions, *Mol Pharm*, 12: 162-70.

Li, Jinghan, Hao Pan, Qingzhuo Ye, Caihong Shi, Xiangrong Zhang, and Weisan Pan. 2020. Carvedilol-loaded polyvinylpyrrolidone electrospun nanofiber film for sublingual delivery, *J Drug Deliv Sci Technol*, 58: 101726.

Lim, Hanpin, Dongyue Yu, and Stephen W Hoag. 2021. Application of near-infrared spectroscopy in detecting residual crystallinity in carbamazepine–Soluplus® solid dispersions prepared with solvent casting and hot-melt extrusion, *J Drug Deliv Sci Technol,* 65: 102713.

Limwikrant, Waree, Aiko Nagai, Yumi Hagiwara, Kenjirou Higashi, Keiji Yamamoto, and Kunikazu Moribe. 2012. Formation mechanism of a new carbamazepine/malonic acid cocrystal polymorph, *Int J Pharm*, 431: 237-40.

Mistry, Pinal, Sarat Mohapatra, Tata Gopinath, Frederick G Vogt, and Raj Suryanarayanan. 2015. Role of the strength of drug–polymer interactions on the molecular mobility and crystallization inhibition in ketoconazole solid dispersions, *Mol Pharm*, 12: 3339-50.

Mohapatra, Debabandya P, Satinder Kaur Brar, Rajeshwar Dayal Tyagi, Pierre Picard, and Rao Y Surampalli. 2014. Analysis and advanced oxidation treatment of a persistent pharmaceutical compound in wastewater and wastewater sludge-carbamazepine, *Sci. Total Environ.*, 470: 58-75.

Mohapatra, Sarat, Subarna Samanta, Khushboo Kothari, Pinal Mistry, and Raj Suryanarayanan. 2017. Effect of polymer molecular weight on the crystallization behavior of indomethacin amorphous solid dispersions, *Cryst. Growth Des.*, 17: 3142-50.

Monschke, Marius, and Karl G Wagner. 2020. Impact of HPMCAS on the dissolution performance of polyvinyl alcohol celecoxib amorphous solid dispersions, *Pharmaceutics*, 12: 541.

Monteagudo, JM, A Durán, R González, and AJ Expósito. 2015. In situ chemical oxidation of carbamazepine solutions using persulfate simultaneously activated by heat energy, UV light, Fe2+ ions, and H2O2, *Appl. Catal. B*, 176: 120-29.

Pudipeddi, Madhu, Erika A Zannou, Madhav Vasanthavada, Aruna Dontabhaktuni, Alan E Royce, Yatindra M Joshi, and Abu TM Serajuddin. 2008. Measurement of surface pH of pharmaceutical solids: a critical evaluation of indicator dye sorption method and its comparison with slurry pH method, *J Pharm Sci*, 97: 1831-42.

Rahman, Ziyaur, Cyrus Agarabi, Ahmed S Zidan, Saeed R Khan, and Mansoor A Khan. 2011. Physico-mechanical and stability evaluation of carbamazepine cocrystal with nicotinamide, *AAPS PharmSciTech*, 12: 693-704.

Rumondor, Alfred CF, and Lynne S Taylor. 2010. Effect of polymer hygroscopicity on the phase behavior of amorphous solid dispersions in the presence of moisture, *Mol Pharm*, 7: 477-90.

Rustichelli, Cecilia, Gianfranco Gamberini, Valeria Ferioli, Maria Cristina Gamberini, R Ficarra, and S Tommasini. 2000. Solid-state study of polymorphic drugs: carbamazepine, *J. Pharm. Biomed*, 23: 41-54.

Sarabu, Sandeep, Venkata Raman Kallakunta, Suresh Bandari, Amol Batra, Vivian Bi, Thomas Durig, Feng Zhang, and Michael A Repka. 2020. Hypromellose acetate succinate based amorphous solid dispersions via hot melt extrusion: Effect of drug physicochemical properties, *Carbohydr. Polym.*, 233: 115828.

Sethia, S, and E Squillante. 2004. Solid dispersion of carbamazepine in PVP K30 by conventional solvent evaporation and supercritical methods, *Int J Pharm*, 272: 1-10.

Singh, Dilpreet, Neena Bedi, and Ashok K Tiwary. 2018. Enhancing solubility of poorly aqueous soluble drugs: Critical appraisal of techniques, *Int. J. Pharm. Investig.*, 48: 509-26.

Solanki, Nayan G, Kyle Lam, Md Tahsin, Suhas G Gumaste, Ankita V Shah, and Abu TM Serajuddin. 2019. Effects of surfactants on itraconazole-HPMCAS solid dispersion prepared by hot-melt extrusion I: miscibility and drug release, *J Pharm Sci*, 108: 1453-65.

Taylor, Lynne S, and George Zografi. 1997. Spectroscopic characterization of interactions between PVP and indomethacin in amorphous molecular dispersions, *Pharm Res*, 14: 1691-98.

Ueda, Keisuke, Kenjirou Higashi, Keiji Yamamoto, and Kunikazu Moribe. 2013. Inhibitory effect of hydroxypropyl methylcellulose acetate succinate on drug recrystallization from a supersaturated solution assessed using nuclear magnetic resonance measurements, *Mol Pharm*, 10: 3801-11.

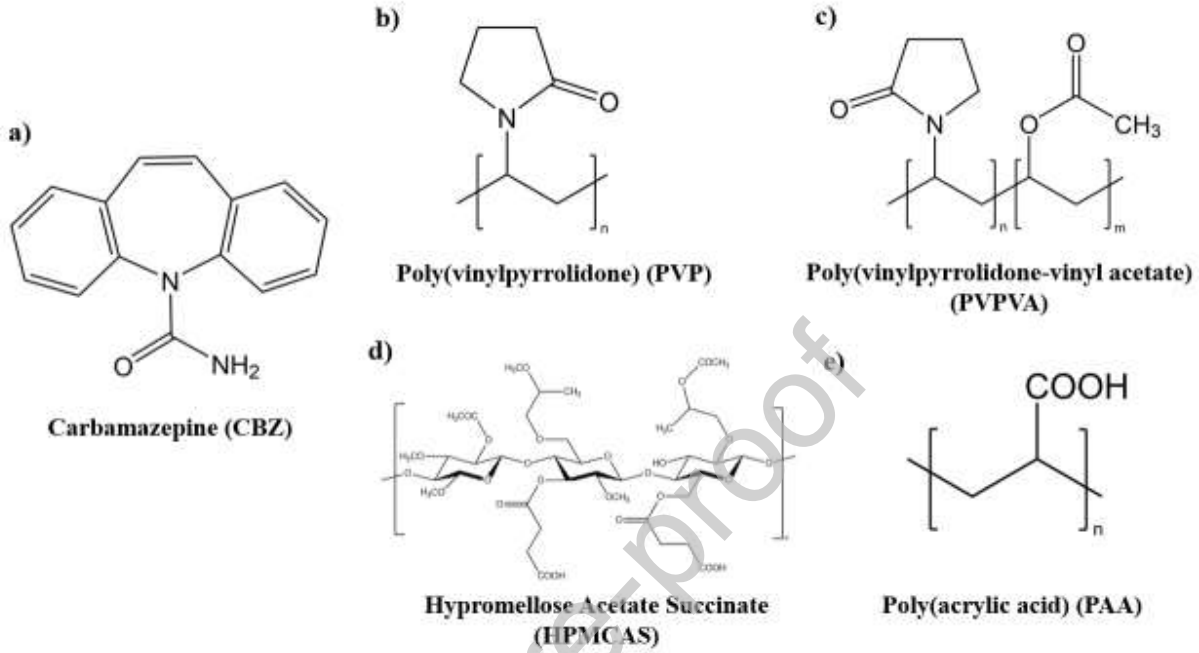

Figure 1. Chemical structures of (a) CBZ, (b) PVP, (c) PVPVA 64, (d) HPMCAS-L, and (e) PAA.

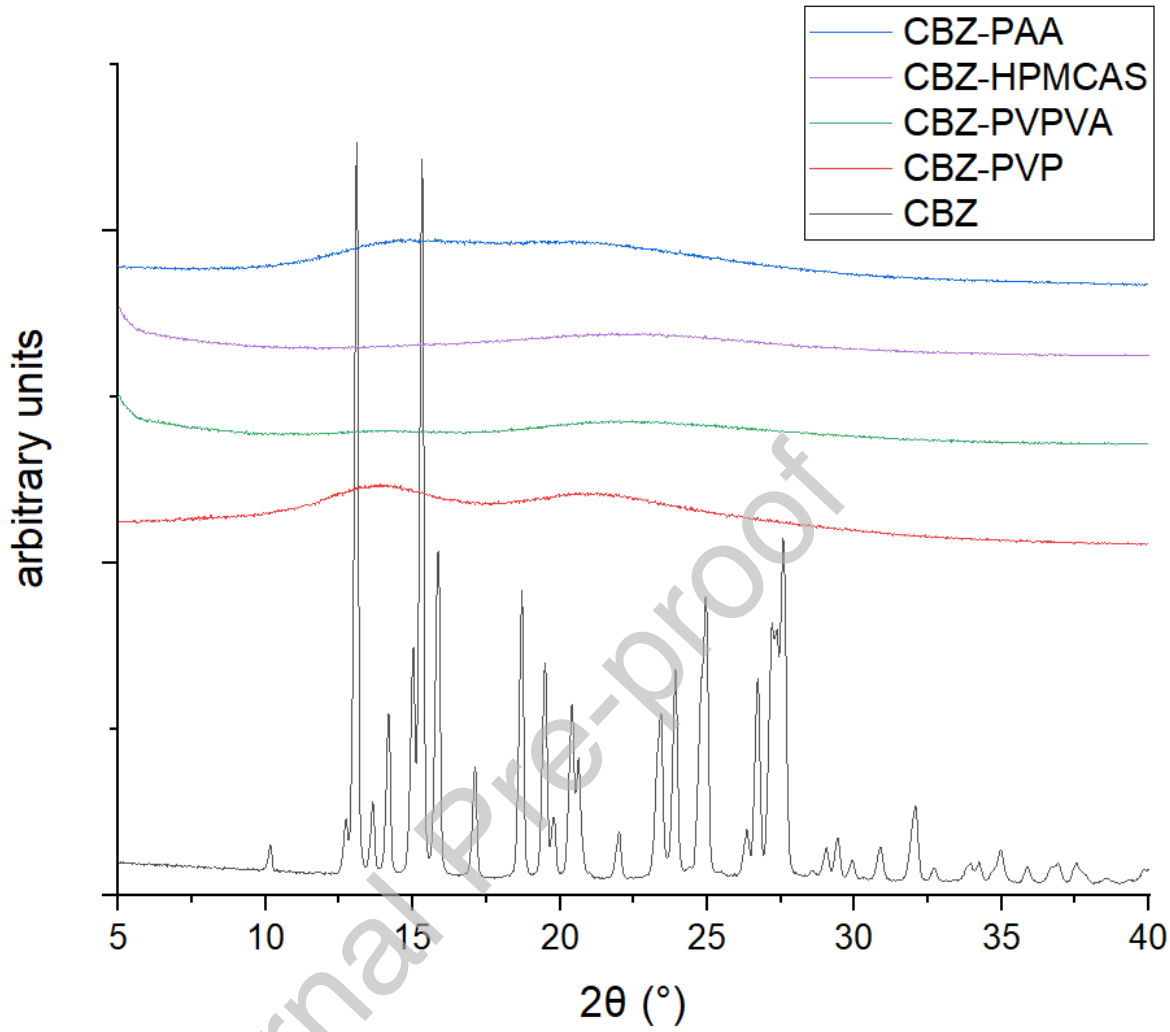

Figure 2. XRD patterns of neat CBZ form III (black), and ASDs of CBZ-PVP (red), CBZ-PVPVA (green), CBZ-HPMCAS (violet), and CBZ-PAA (blue).

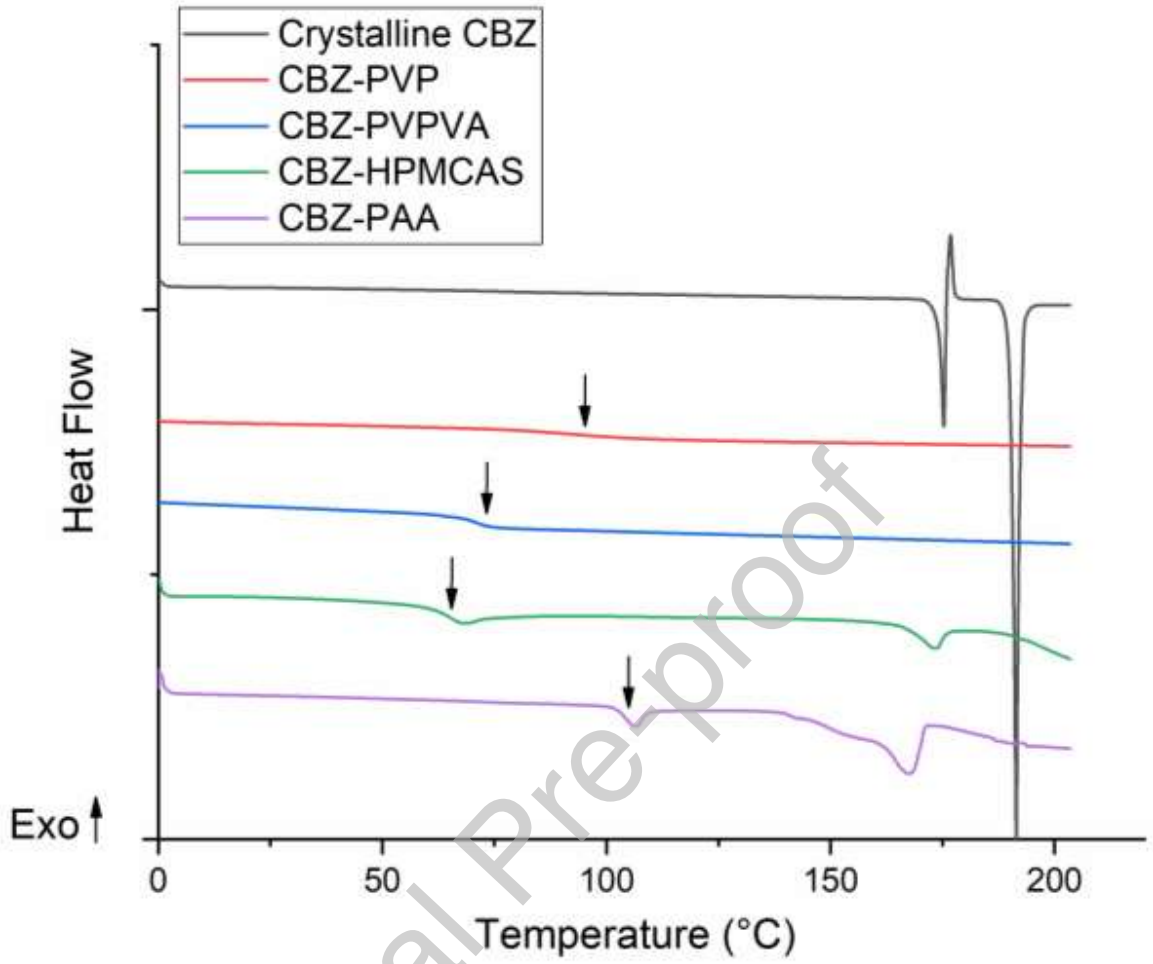

Figure 3. DSC thermograms of CBZ form III (black), and ASDs of CBZ-PVP (red), CBZ-PVPVA (blue), CBZ-HPMCAS (green), and CBZ-PAA (violet). The glass transition temperatures were determined at the midpoint of the transition and marked with arrows.

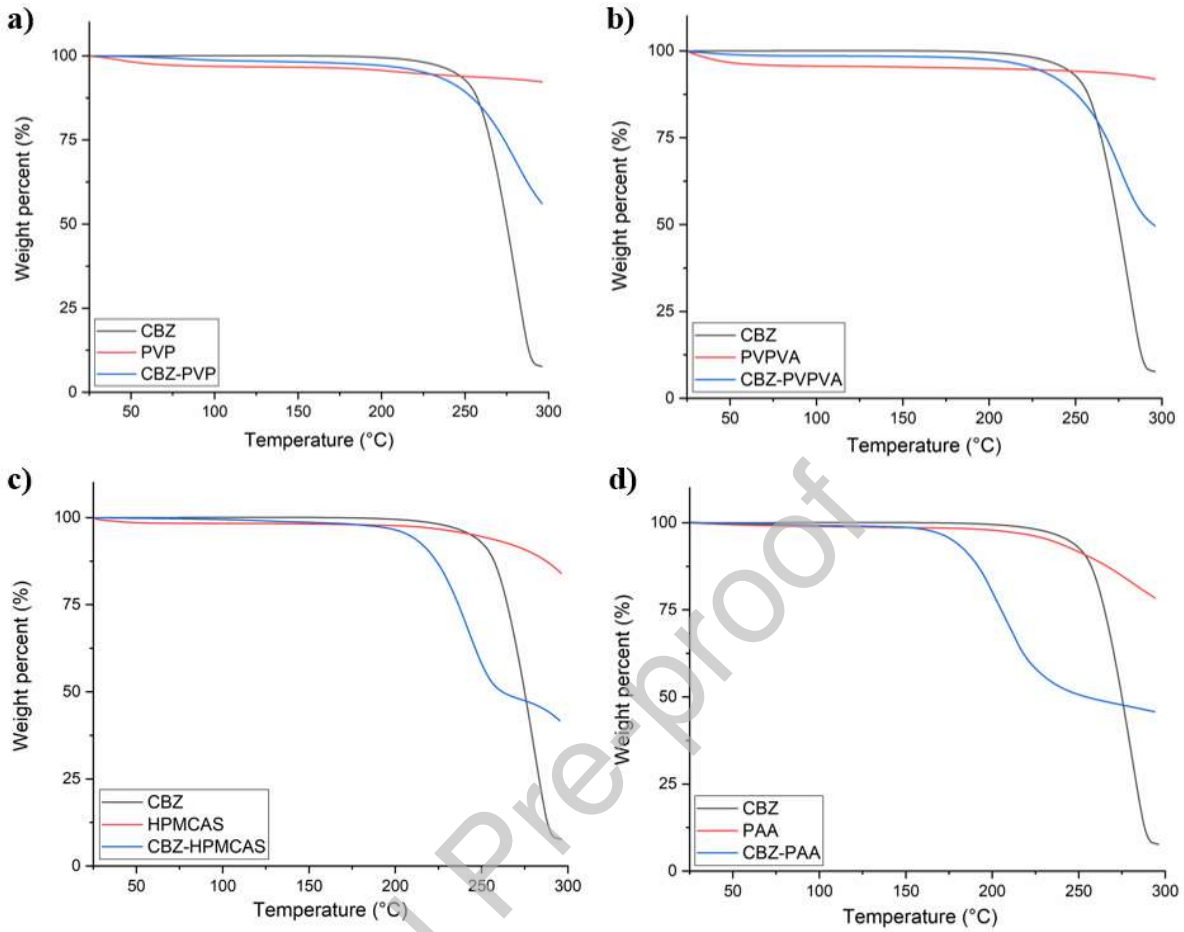

Figure 4. TGA results of crystalline CBZ (black), polymers (red), and CBZ ASDs (blue): panel a) PVP, b) PVPVA, c) HPMCAS, and d) PAA.

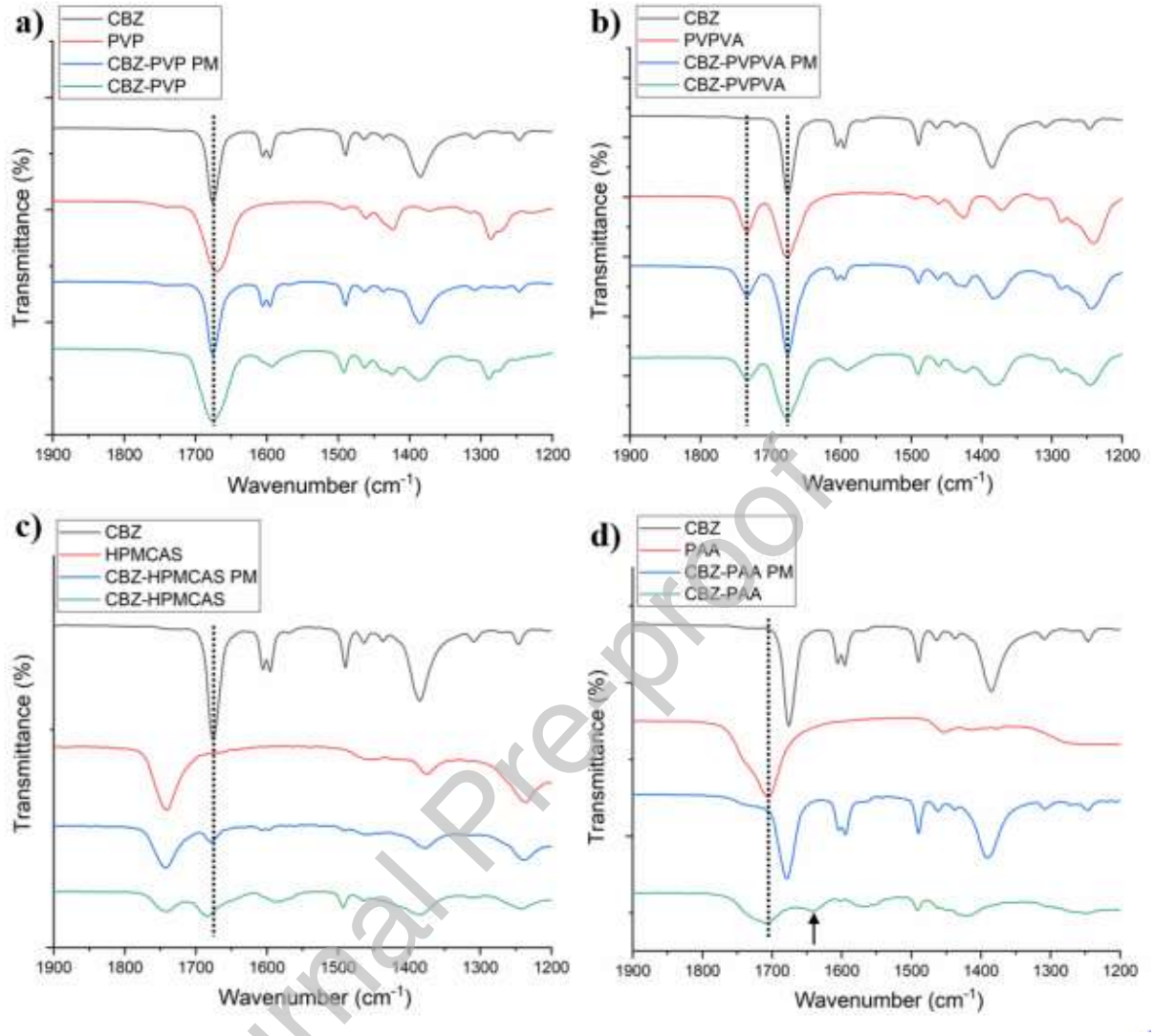

Figure 5. FTIR spectra of the crystalline CBZ (black), polymers (red), physical mixtures (PMs) (blue), ASDs (green): panel a) PVP, b) PVPVA, c) HPMCAS, and d) PAA systems with the wavelength from 1900 to 1200 cm^{-1}.

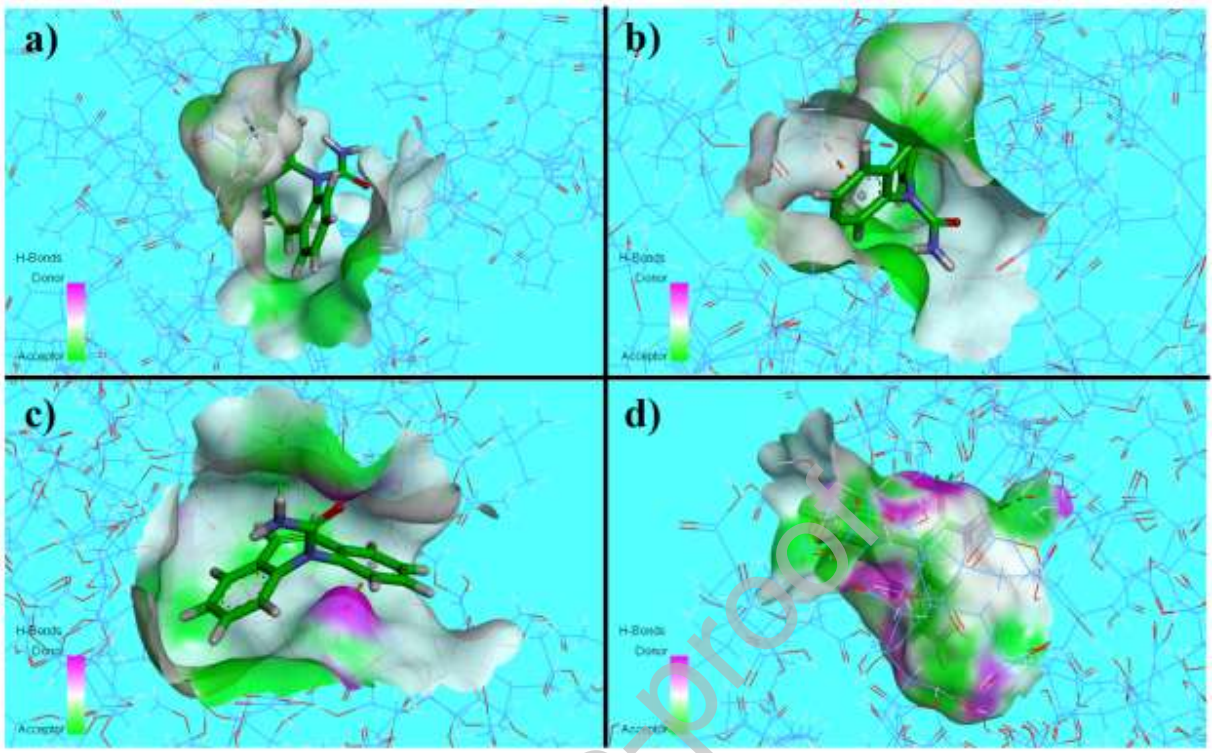

Figure 6. Close-up view of molecular structures of a) CBZ-PVP, b) CBZ-PVPVA, c) CBZ-HPMCAS, and d) CBZ-PAA ASDs. The interacting domains are presented with a hydrogen bond receptor surface. Hydrogen bonds and hydrophobic forces are described in the green and orange dash-line, respectively.

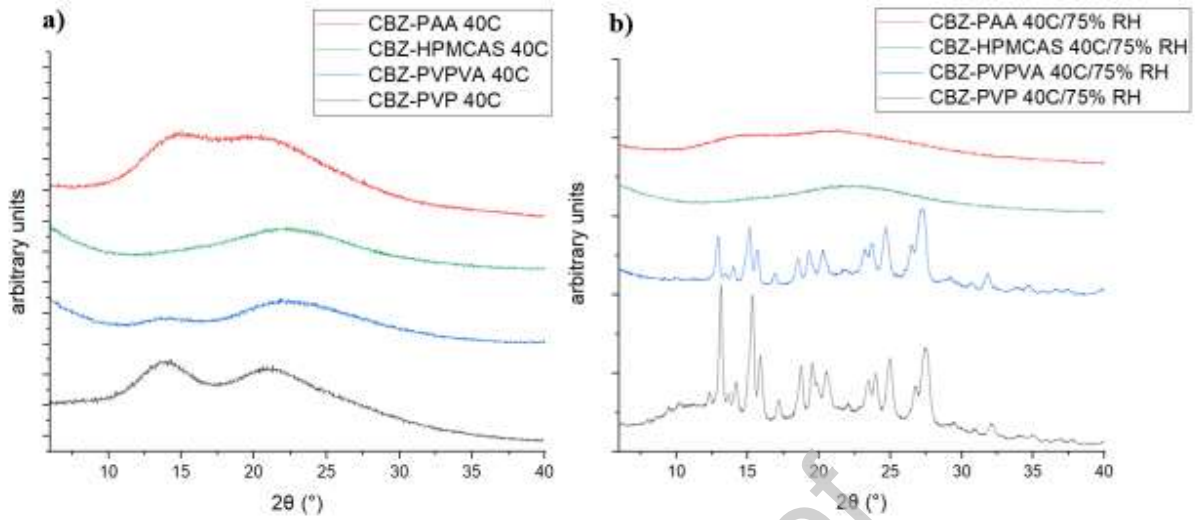

Figure 7. XRD patterns of PVP (black), PVPVA (blue), HPMCAS (green), and PAA (red) ASDs after 8-week storage at a) 40 ° C dry condition and b) 40 ° C/75 % RH.

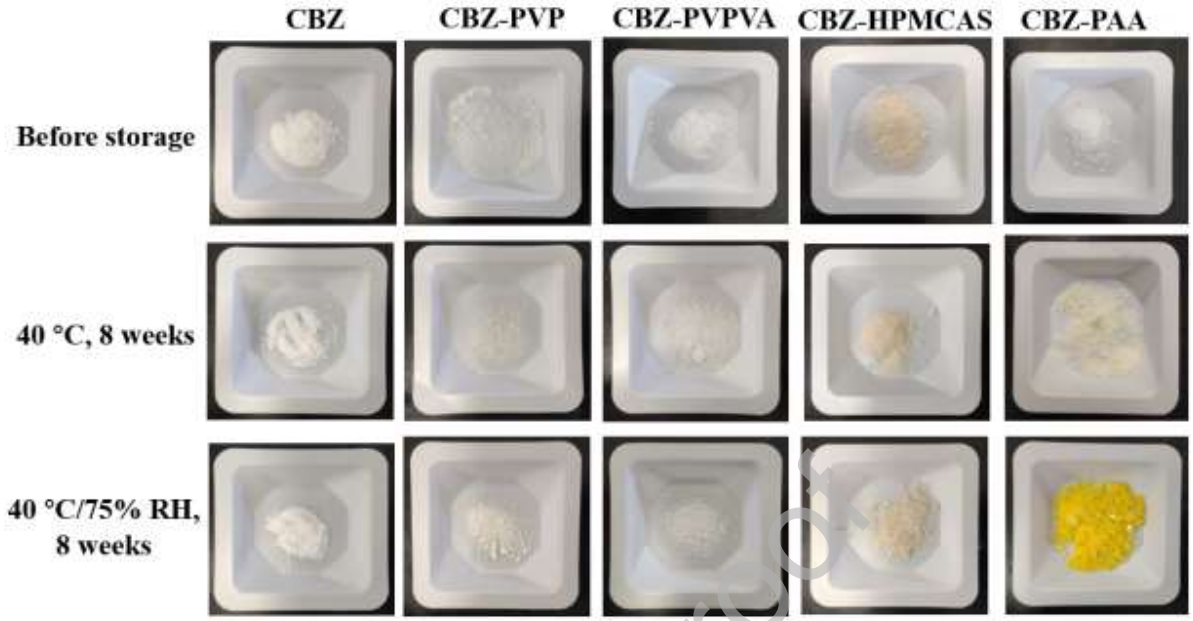

Figure 8. The appearance of crystalline CBZ and ASDs before and after storage at 40 ° C dry and 40 ° C/75% RH conditions.

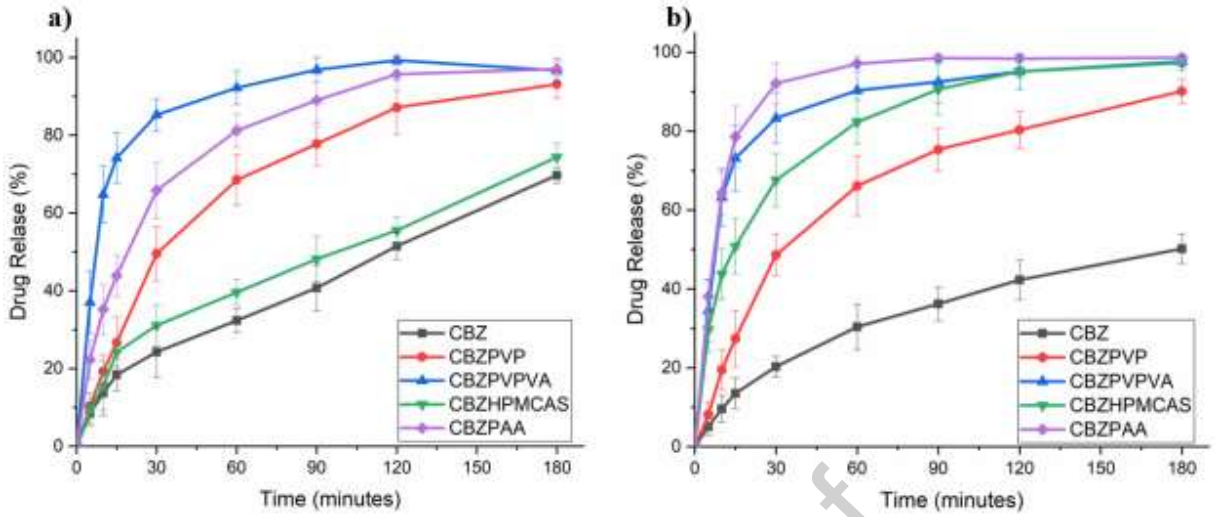

Figure 9. Dissolution profiles of crystalline CBZ and CBZ ASDs in a) pH 1.2 and b) pH 6.8 buffers at 37° C.

Table 1. The microenvironmental pH values of CBZ, polymers, and ASDs.

Drug and Polymers	pH	ASDs	pH

CBZ	8.95 ± 0.04	--	--
PVP	5.03 ± 0.11	CBZ-PVP	4.98 ± 0.23
PVPVA	5.83 ± 0.08	CBZ-PVPVA	6.11 ± 0.18
HPMCAS	3.81 ± 0.08	CBZ-HPMCAS	4.67 ± 0.21
PAA	2.76 ± 0.13	CBZ-PAA	2.98 ± 0.14

Table 2. Percentage of CBZ remained in the neat CBZ and CBZ ASDs after an 8-week storage

	CBZ (%)	PVP ASD (%)	PVPVA ASD (%)	HPMCAS ASD (%)	PAA ASD (%)
40 °C/dry	96.66 ± 0.85	97.78 ± 0.49	97.52 ± 0.54	97.39 ± 0.05	96.57 ± 0.02
40 °C/75 % RH	96.33 ± 0.56	95.92 ± 0.48*	97.77 ± 0.11*	95.35 ± 0.42	87.11 ± 1.10

* Sample recrystallized during storage

GA